Available online at www.sciencedirect.com
ScienceDirect
Trans. Nonferrous Met. Soc. China 34(2024) 3737−3748
Transactions of Nonferrous Metals Society of China
www.tnmsc.cn

Synergistic extraction and separation of valuable elements from high-alumina fly ash with carbochlorination method

Long WANG[1], Xin-xin ZHAO[1], Zi-mu ZHANG[2], Ting-an ZHANG[1], Guo-zhi LÜ[1], Zhi-he DOU[1], Ai-chun ZHAO[3], Xi-yu ZHANG[1]

1. Key Laboratory for Ecological Utilization of Multimetallic Mineral of Ministry of Education, Northeastern University, Shenyang 110819, China;
2. College of Mechanical Engineering, Shenyang University of Chemical Technology, Shenyang 110142, China;
3. School of Materials Science and Engineering, Taiyuan University of Science and Technology, Taiyuan 030024, China

Received 22 April 2023; accepted 15 November 2023

Abstract: A novel process was proposed for synergistic extraction and separation of valuable elements from high-alumina fly ash. A thermodynamic analysis revealed that to achieve effective carbochlorination, it is crucial to conduct carbochlorination of the fly ash within the temperature range from 700 to 1000 °C. The experimental results demonstrated that under the optimal conditions, the carbochlorination efficiency for Al, Si, Ca, Ti, and Mg exceeded 81.18%, 67.62%, 58.87%, 82.15%, and 59.53%, respectively. The XRD patterns indicated that Al and Si in the mullite phase ($Al_6Si_2O_{13}$) were chlorinated during the carbochlorination process, resulting in the formation of mullite mesophases ($Al_{4.75}Si_{1.25}O_{9.63}$ and $Al_{1.83}Si_{1.08}O_{4.85}$). After the carbochlorination process, Al was accumulated as $AlCl_3$ in the condenser, while $SiCl_4$ and $TiCl_4$ were enriched in the exhaust gas, and $CaCl_2$, $MgCl_2$, and unreacted oxides remained in the residue for further recycling.

Key words: high-alumina fly ash; carbochlorination; thermodynamics; synergistic extraction; mechanism

1 Introduction

Given its high alumina content of nearly 50%, high-alumina fly ash is a significant alternative resource to bauxite [1]. High-alumina coal is primarily found in Shanxi, Inner Mongolia, and Ningxia in China. The proven resources of high-alumina coal are 50 billion tons, with prospective resources exceeding 100 billion tons [2]. Burning high-alumina coal can potentially produce approximately 14 billion tons of high-alumina fly ash [3] . The annual discharge of high-alumina fly ash has exceeded 60 million tons, with the accumulated stock surpassing 300 million tons [4]. From an environmental perspective, the accumulation of high-alumina fly ash had led to significant ecological contamination [5]. However, from a resource perspective, high-alumina fly ash contains abundant resources, including aluminum, silicon, gallium, lithium, scandium, and other elements. Therefore, it can be considered a significant “urban mineral” resource [6].

The mineral composition in high-alumina fly ash is closely associated with the comprehensive utilization level. The primary mineral components of high-alumina coal include kaolinite, quartz, pyrite, and other minerals [7,8]. A phase transformation of kaolinite occurs during the combustion process of high-alumina coal as the combustion temperatures vary [9] :

Corresponding author: Ting-an ZHANG, Tel: +86-13840205331, E-mail: zta2000@163.net
DOI: 10.1016/S1003-6326(24)66637-9

550 °C: $Al_2O_3·2SiO_2·2H_2O$ (kaolinite)→
$Al_2O_3·2SiO_2$ (metakaolin)+$2H_2O$ (1)

850 °C: $Al_2O_3·2SiO_2$→
$Al_2O_3·SiO_2$ (sillimanite)+SiO_2 (2)

950 °C: $Al_2O_3·SiO_2$→
SiO_2+$\gamma·Al_2O_3$ (3)

1000−1100 °C: $3Al_2O_3·2SiO_2$→
$3Al_2O_3·2SiO_2$ (mullite) (4)

High-alumina fly ash is classified as circulating fluidized bed fly ash (referred to as CFB fly ash) or pulverized coal furnace fly ash (referred to as PC fly ash) based on the different types of combustion furnaces used [10]. The combustion temperature range of a circulating fluidized bed is 850−950 °C. Additionally, the predominant phases in CFB fly ash are amorphous silicon, alumina, sillimanite, and a minor proportion of mullite [11]. However, the combustion temperatures of pulverized coal furnaces range from 1250 to 1450 °C, and the phases in PC fly ash include mullite, corundum, quartz, and other crystalline minerals [12]. In addition, the aluminum, silicon, gallium, lithium, scandium, and other elements in the PC fly ash are encapsulated within spherical glass particles [13]. The complex phase structure and the spherical shells in PC fly ash pose challenges for extraction [14].

The utilization methods for fly ash can be categorized into alkali and acid methods [15,16]. The alkali process primarily comprises lime sintering, alkali lime sintering, and prior desiliconization alkali lime sintering [17]. The lime sintering method is not cost-effective due to the high energy consumption, low alumina dissolution rate, and excessive slag production. By incorporating sodium carbonate into the limestone sintering process, the alkali lime sintering method reduced the energy consumption and minimized waste residue discharge [18]. However, this method also led to augmented alkali consumption and diminished alumina extraction efficiency, resulting in a suboptimal economic benefit. In the prior desiliconization process, sodium hydroxide was reacted with the amorphous silica in the high-alumina fly ash, thereby enhancing the aluminum−silicon ratio of the fly ash. Then, alkali lime sintering was used to extract the alumina from the prior desiliconization residues. After several years of industrial operation, this method was ultimately discontinued due to its exorbitant operating cost.

The acid process primarily involves the use of sulfuric acid and hydrochloric acid to separate the aluminum and silicon in fly ash [18]. However, these methods cannot effectively disrupt the intricate phase structure of the aluminum−silicon in fly ash. Therefore, an external field is often applied to improving the extraction process [19,20]. Another key challenge in the acid method arises from the purification, evaporation, and crystallization of aluminum chloride [21]. The acid method facilitates efficient utilization of multiple elements from high-alumina fly ash more than the alkali method [22,23]. However, the evaporation and crystallization of aluminum chloride consumes a substantial amount of energy and the alumina products fail to meet the quality requirements for aluminum electrolysis [24].

In conclusion, these conventional methods are plagued by environmental contamination and exorbitant operating expenses. The carbochlorination method presents a promising approach for high-alumina fly ash, with advantages such as enhanced conversion efficiency, minimal residue discharge, and utilization of multiple elements [25−29]. The carbochlorination of fly ash generally involves two procedures: carbochlorination and purification. The carbochlorination process involves the conversion of aluminum, silicon, and other oxides into chloride phases. After the carbochlorination process, washing is implemented to recover valuable chlorides such as $CaCl_2$, $MgCl_2$, and LiCl. The unreacted oxides are blended with the raw materials and reintroduced into the carbochlorination process, ensuring "zero waste" discharge. The purification process is a mature technique for refining $AlCl_3$, $SiCl_4$, and other metal chlorides. $AlCl_3$ is widely used as a catalyst in various synthetic organic processes. $SiCl_4$ plays a crucial role in the production of high-purity silicon and ethyl silicate.

This study employed the carbochlorination method to extract valuable metals from PC fly ash. A thermodynamic analysis was employed to estimate the carbochlorination principles of the fly ash. The objective of the single-factor experiments was to determine the optimal conditions and elucidate the mechanism for the fly ash carbochlorination.

2 Experimental

2.1 Materials

The fly ash and carbon used in this study were sourced from a thermal power plant in Inner Mongolia, China. The contents of Al_2O_3, SiO_2, MgO, TiO_2, and CaO were analyzed by ICP (Optima 8300DV, PE, USA), and the chemical components are presented in Table 1. The blended gas consisted of nitrogen (N_2 > 99.9%) and chlorine (Cl_2 > 99.8%).

Table 1 Chemical composition of high-alumina fly ash used in this study (wt.%)

Al_2O_3	SiO_2	MgO	TiO_2	CaO	Others
48.39	38.73	0.40	1.74	2.65	8.09

2.2 Methods

2.2.1 Carbochlorination

A schematic diagram of the experimental setup for carbochlorination process is provided in Fig. 1.

The fly ash, carbon, and binder were mixed in a particular ratio and pelletized to a specific size with a disk granulating machine (Zhengzhou Machinery Manufacturing, Zhengzhou, China). The fine pellets were dried at 90 °C for 24 h. The dried pellets were arranged within a packed bed reactor (TJZ, Tianjin Zhonghuan Furnace Corp., China), which was equipped with a separation apparatus for the carbochlorination product. The carbochlorination experiment was conducted at a predetermined temperature for a specific duration, employing various nitrogen and chlorine gas compositions.

2.2.2 Water leaching

The carbochlorination residues were leached with a liquid-to-solid ratio of 5:1, a temperature of 60 °C, and time of 1 h. The leaching residues were subsequently separated with a circulating water vacuum pump (SHZ-DIII, Henan Yucheng apparatus, China) and analyzed by ICP. The carbochlorination efficiency (η) for the major constituents in the fly ash was determined with Eq. (5):

$$\eta=(1-m_1/m_0)\times100\% \quad (5)$$

where m_0 and m_1 are the mass of elements in the pellet before carbochlorination and in the residues after carbochlorination, respectively.

SEM (SU−8010, Japan) was employed to examine the morphologies of the carbochlorination residues and the products. The phase compositions of the residues and the products were examined by XRD (PW3040/60, Philips, Netherlands).

3 Results and discussion

3.1 Carbochlorination principle of principal components in fly ash

The melting points, boiling points, and vapor pressures of the carbochlorination products are illustrated in Fig. 2.

In Fig. 2, the melting points, boiling points, and vapor pressures of the carbochlorination products confirmed the viability of separating the carbochlorination products via condensation. Moreover, it is imperative to assess the viability of using carbochlorination of the primary constituents in fly ash. Based on the use of 1 mol Cl_2 in the carbochlorination reaction, the potential carbochlorination reactions and standard Gibbs free energy changes are presented in Table 2 and Fig. 3.

In Fig. 3, the standard Gibbs free energy changes for the potential reactions of the principal components in the fly ash were negative at temperatures

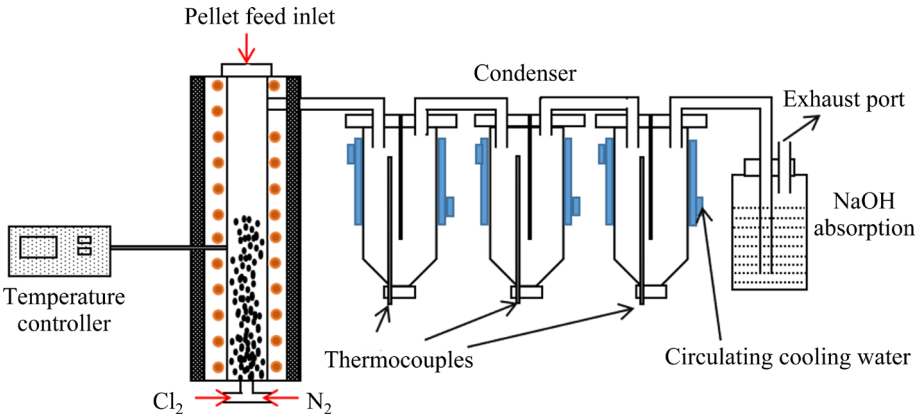

Fig. 1 Schematic diagram showing experimental setup for carbochlorination

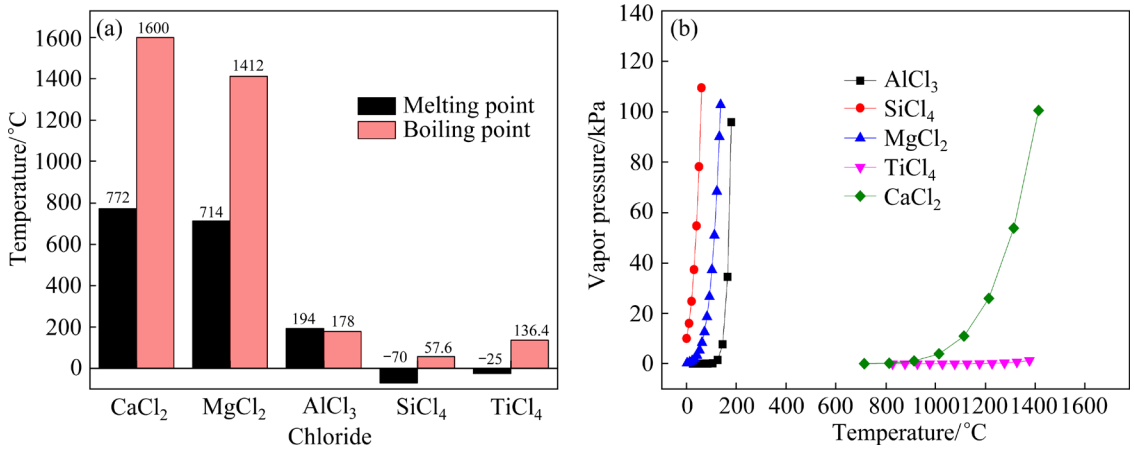

Fig. 2 Melting points and boiling points (a), and vapor pressures (b) of carbochlorination products

Table 2 Potential reactions and standard Gibbs free energy changes for carbochlorination of fly ash

No.	Potential reaction of M (M= Al, Si, Ti, Mg, Ca)−O−Cl system	$\Delta G^{\ominus}$/(kJ·mol^{-1})	
		600 °C	900 °C
1	$1/13Al_6Si_2O_{13}+Cl_2(g)+1/2C=1/2CO_2(g)+6/13AlCl_3(g)+2/13SiCl_4(g)$	−92.43	−108.79
2	$1/13Al_6Si_2O_{13}+Cl_2(g)+C=CO(g)+6/13AlCl_3(g)+2/13SiCl_4(g)$	−83.63	−126.26
3	$1/3Al_2O_3+Cl_2(g)+1/2C=1/2CO_2(g)+2/3AlCl_3(g)$	−91.22	−111.683
4	$1/3Al_2O_3+Cl_2(g)+C=CO(g)+2/3AlCl_3(g)$	−82.43	−129.16
5	$1/2SiO_2+Cl_2(g)+1/2C=1/2CO_2(g)+1/2SiCl_4(g)$	−95.15	−102.27
6	$1/2SiO_2+Cl_2(g)+C=CO(g)+1/2SiCl_4(g)$	−86.35	−119.74
7	$1/2TiO_2+Cl_2(g)+1/2C=1/2CO_2(g)+1/2TiCl_4(g)$	−133.42	−141.95
8	$1/2TiO_2+Cl_2(g)+C=CO(g)+1/2TiCl_4(g)$	−124.62	−159.42
9	$MgO+Cl_2(g)+1/2C=1/2CO_2(g)+MgCl_2$	−194.67	−190.49
10	$MgO+Cl_2(g)+C=CO(g)+MgCl_2$	−185.88	−207.97
11	$CaO+Cl_2(g)+1/2C=1/2CO_2(g)+CaCl_2$	−317.59	−309.75
12	$CaO+Cl_2(g)+C=CO(g)+CaCl_2$	−308.80	−327.23

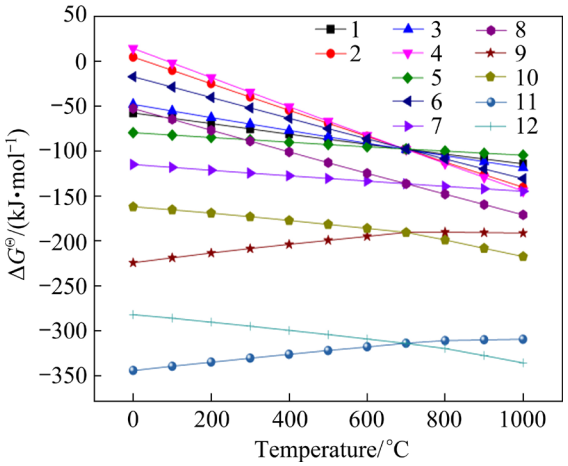

Fig. 3 Standard Gibbs free energy changes for carbochlorination of fly ash corresponding potential reactions in Table 2 at 0−1000 °C

of 200−1000 °C, which showed that these reactions proceeded in the forward direction. The standard Gibbs free energies for carbochlorination of other compounds were relatively insignificant compared to those for chlorination of MgO and CaO, indicating a higher priority for the carbochlorination reactions of MgO and CaO over those of $Al_6Si_2O_{13}$, Al_2O_3, SiO_2, and TiO_2. The standard Gibbs free energies of $Al_6Si_2O_{13}$ and Al_2O_3 were relatively positive over the temperature of 0−737 °C compared to that of SiO_2, indicating that higher temperatures drove the carbochlorination reactions of $Al_6Si_2O_{13}$ and Al_2O_3. Furthermore, within the temperature of 737−1000 °C, the standard Gibbs free energy changes for all compounds in the fly ash exhibited significantly

more negative values when CO was produced as a reaction product rather than CO_2. The thermodynamic analyses suggested that the temperatures of 700−1000 °C are crucial for optimizing the carbochlorination efficiency.

3.2 Carbochlorination efficiency of high-alumina fly ash

Carbochlorination experiments with fly ash were conducted to evaluate the impacts of the gas flow rate, time, carbon content, temperature, and proportion of Cl_2 in the blended introducing gas.

3.2.1 Effect of gas flow rate

The effect of the gas flow rate was investigated with gas flow rates ranging from 0.10 to 0.35 L/min, a temperature of 950 °C, a time of 60 min, pellet diameters ranging from 4 to 6 mm, chlorine proportion of 100%, and a carbon content of 27.0 wt.%. The carbochlorination efficiency and XRD patterns of fly ash at various flow rates are illustrated in Fig. 4.

As shown in Fig. 4(a), the gas flow rate had a significant influence on the carbochlorination efficiency of Al, Si, Ca, Ti, and Mg in fly ash. The results showed an increasing trend as the gas flow rate increased from 0.10 to 0.35 L/min. The optimal carbochlorination processes for Al, Si, Ca, Ti, and Mg were achieved with a gas flow rate of 0.35 L/min, and the efficiencies were 69.65%, 54.55%, 76.02%, 73.44%, and 49.46%, respectively. In Fig. 4(b), the carbochlorination residues contained a mullite mesophase ($Al_{4.75}Si_{1.25}O_{9.63}$), alumina ($Al_2O_3$), and silica ($SiO_2$) at gas flow rates of 0.10 and 0.20 L/min. The carbochlorination residues primarily consisted of a mullite mesophase ($Al_{1.83}Si_{1.08}O_{4.85}$), alumina ($Al_2O_3$), and silica ($SiO_2$) when the gas flow rate reached 0.30 L/min. With increased gas flow rates at 0.30 and 0.35 L/min, the amount of the mullite mesophase ($Al_{4.56}Si_{1.44}O_{9.72}$) diminished. In contrast, a new mullite mesophase ($Al_{1.83}Si_{1.08}O_{4.85}$) emerged, offering a potential explanation for the improved carbochlorination outcome for aluminum and silicon.

However, the pellets were pulverized when the gas flow rate exceeded a certain threshold. Rapid pulverization of the pellets deteriorated the gas–solid reaction conditions and led to the discharge of fly ash from the reaction zone with the gas flow. Hence, a suitable gas flow rate of 0.30 L/min was used in the subsequent experiments.

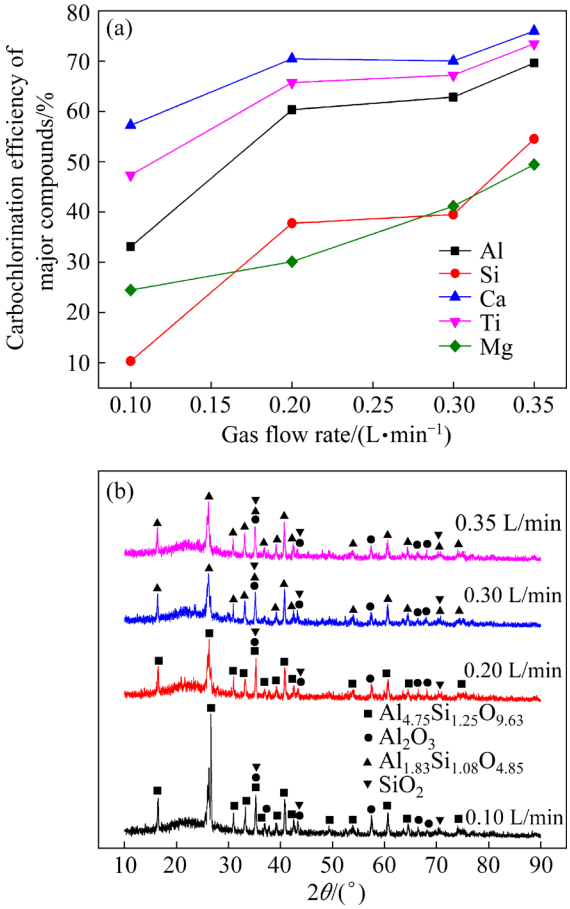

Fig. 4 Carbochlorination efficiency (a) and XRD patterns (b) of fly ash at various flow rates

3.2.2 Effect of time

The effect of time on the carbochlorination efficiency and XRD patterns of fly ash are shown in Fig. 5, and the following conditions were used: time of 15 to 120 min, temperature of 950 °C, carbon content of 27.0 wt.%, pellet diameters ranging from 4 to 6 mm, and gas flow rate of 0.30 L/min with a chlorine proportion of 100%.

The carbochlorination reactions of Al, Si, Ca, Ti, and Mg in the fly ash exhibited increasing efficiency with increasing reaction time from 15 to 120 min. The optimum carbochlorination efficiency was realized after 120 min, resulting in efficiencies of 79.31%, 63.89%, 82.76%, 81.61%, and 54.99%, respectively (Fig. 5(a)). The carbochlorination efficiencies of Al, Ca, and Ti were significantly superior to those of Si and Mg with the extended carbochlorination time. The principal phases observed in the carbochlorination residues were mullite mesophase ($Al_{4.75}Si_{1.25}O_{9.63}$, $Al_{1.83}Si_{1.08}O_{4.85}$), alumina ($Al_2O_3$), and silica ($SiO_2$), as shown in Fig. 5(b). The mullite phase in the fly ash was

transformed from $Al_6Si_2O_{13}$ to $Al_{1.83}Si_{1.08}O_{4.85}$ with extended carbochlorination time from 15 to 120 min. The intensities of the peaks at 16.35°, 26.18°, and 40.75° for the mullite mesophase exhibited significant decrease, indicating that the carbochlorination process continuously disrupted the crystal structure of the mullite phase in the fly ash.

The above statement explains the carbochlorination efficiency of the fly ash as a function of increasing carbochlorination time. Due to the continuous consumption of carbon in the pellets, the limited amount of carbon inhibited carbochlorination of the fly ash with extended time. Therefore, the subsequent carbochlorination experiments were run for 60 min.

3.2.3 Effect of carbon content

The effect of carbon content was investigated with the following conditions: temperature of 950 °C, time of 60 min, pellet diameter ranging from 4 to 6 mm, gas flow rate of 0.30 L/min with a chlorine proportion of 100%, and carbon contents of 20.4, 23.9, 27.0 and 29.9 wt.%. The effects of carbon content on the carbochlorination efficiency and XRD patterns of fly ash are shown in Fig. 6.

Carbochlorination of the fly ash was significantly affected by the carbon content in the pellets, as shown in Fig. 6(a). The carbochlorination efficiency for Al, Si, Ca, Ti, and Mg in the fly ash exhibited rapid increase from 50.86%, 27.58%, 9.84%, 52.09% and 15.04% (20.4 wt.% carbon content) to 81.19%, 67.62%, 58.88%, 82.15% and 59.53% (27.0 wt.% carbon), followed by subsequent decrease with increase of carbon content from 27.0 wt.% to 29.0 wt.%. The incomplete reactions with low carbon constituted suboptimal efficiency. Carbochlorination of the fly ash reached the maximum efficiency with a carbon content of 27.0 wt.%, where it approached the theoretical carbon requirement. A thermodynamic analysis revealed that a high carbon content elevated the partial pressures of CO and CO_2 while simultaneously reducing the partial pressure of Cl_2. This inhibited carbochlorination of the primary components in the fly ash.

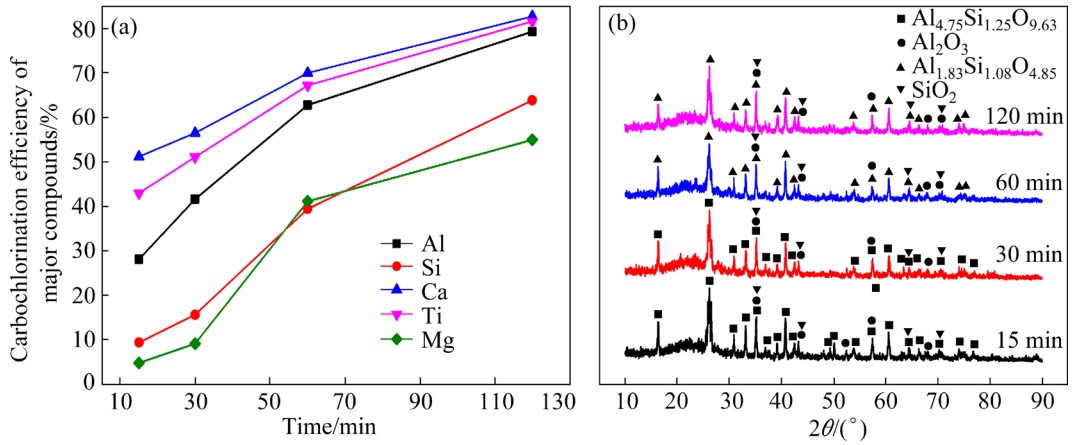

Fig. 5 Carbochlorination efficiency (a) and XRD patterns (b) of fly ash determined at various time

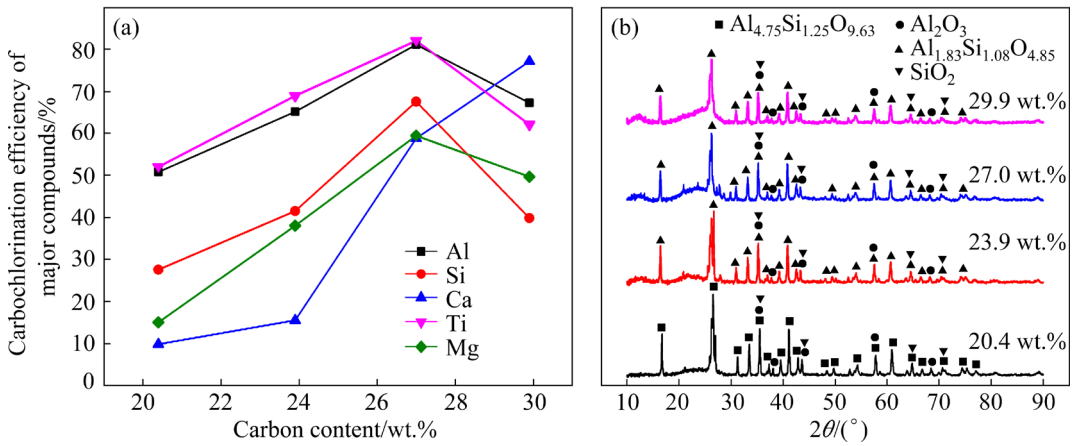

Fig. 6 Carbochlorination efficiency (a) and XRD patterns (b) of fly ash with various carbon contents

As shown in Fig. 6(b), the carbochlorination residues primarily consisted of a mullite mesophase ($Al_{4.75}Si_{1.25}O_{9.63}$), alumina ($Al_2O_3$), and silica ($SiO_2$) with a carbon content of 20.4 wt.%. A higher carbon content in the pellets resulted in disappearance of the diffraction peaks associated with the mullite mesophase ($Al_{4.75}Si_{1.25}O_{9.63}$), while a new mullite mesophase ($Al_{1.83}Si_{1.08}O_{4.85}$) emerged, which explained the improved carbochlorination efficiency of the fly ash.

3.2.4 Effect of temperature

The effect of temperature was determined with temperature ranging from 800 to 950 °C, reactions time of 60 min, pellet diameter ranging from 4 to 6 mm, gas flow rate of 0.30 L/min with a chlorine proportion of 100%, and carbon content of 27.0 wt.%. The results are shown in Fig. 7.

The carbochlorination efficiency of Al, Si, Ca, Ti, and Mg in the fly ash increased as the temperature increased, as depicted in Fig. 7(a). The carbochlorination efficiencies for Al, Si, Ca, Ti, and Mg in the fly ash increased from 50.22%, 34.39%, 28.04%, 40.36% and 8.79% at 800 °C to 81.18%, 67.62%, 58.87%, 82.15% and 59.53% at 950 °C, respectively, which was consistent with the thermodynamic predictions. The XRD patterns for the carbochlorination residues produced at various temperatures are illustrated in Fig. 7(b). The new phase appearing in the carbochlorination residues after heating at 800 °C was identified as $MgSiO_3$, indicating that some of the MgO and SiO_2 were converted into $MgSiO_3$ at this temperature. The diffraction peaks for the mullite mesophase ($Al_{1.83}Si_{1.08}O_{4.85}$) were observed for the residues produced at a carbochlorination temperature of 900 °C. The increased carbochlorination temperature from 900 to 950 °C resulted in diffraction peaks for the mullite mesophase ($Al_{1.83}Si_{1.08}O_{4.85}$) in the residues, indicating that aluminum and silicon were extracted from the mullite phase ($Al_6Si_2O_{13}$) in the fly ash during carbochlorination. Hence, subsequent experiments were conducted at 950 °C.

3.2.5 Effect of Cl_2 proportion in blended introduction gas

Figure 8 shows the effect of Cl_2 proportion in the introduced gas ranging from 60% to 100% under conditions of temperature of 950 °C, time of 60 min, pellet diameters of 4−6 mm, gas flow rate of 0.30 L/min, and carbon content of 27.0 wt.%.

The carbochlorination efficiencies for Al, Si, Ca, Ti, and Mg in the fly ash exhibited increasing trends and reached the maximum efficiency of 81.18%, 67.62%, 58.87%, 82.15%, and 59.53%, respectively, when the proportion of Cl_2 was 100%, as shown in Fig. 8(a). The XRD patterns of the carbochlorination residues produced with varying chlorine gas proportions are presented in Fig. 8(b). The main constituents in the residues included mullite mesophase ($Al_{4.75}Si_{1.25}O_{9.63}$, $Al_{1.83}Si_{1.08}O_{4.85}$), alumina ($Al_2O_3$), and silica ($SiO_2$). However, with increased proportions of Cl_2 in the introduced gas, diffraction peaks for the mullite mesophase ($Al_{4.75}Si_{1.25}O_{9.63}$) became indiscernible, whereas those for the mullite mesophase ($Al_{1.83}Si_{1.08}O_{4.85}$) were apparent. The increased proportion of Cl_2 improved the carbochlorination efficiency, thereby facilitating the recovery of valuable metals from the fly ash. Subsequent experiments showed that it was advisable to maintain a Cl_2 proportion of 100% in the introduced gas.

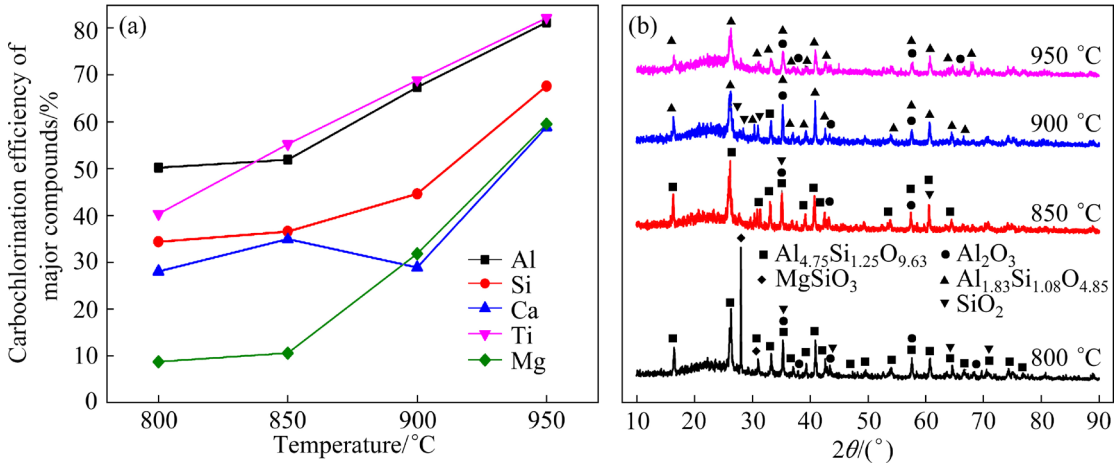

Fig. 7 Carbochlorination efficiency (a) and XRD patterns (b) of fly ash at various temperatures

3.3 Morphologies of carbochlorination residues

The morphologies of the carbochlorination residues were examined by SEM to investigate carbochlorination of the fly ash for different time.

Figure 9(a) shows image of the residue surfaces after carbochlorination for 15 min. The residues exhibited textured surfaces containing crevices and holes. It is worth noting that carbochlorination of the fly ash was not completed and predominantly occurred on the surface of the fly ash, which was consistent with both the carbochlorination efficiency of the fly ash and the XRD results after 15 min. The roughness of the particle surfaces increased as the time increased from 15 to 60 min, as shown in Figs. 9(b) and (c). The carbochlorination reaction of the fly ash progressed from the surfaces toward the interiors of the particles. The carbochlorination residues produced at 120 min exhibited incomplete spherical particles with hollow spherical shell structures, as shown in Fig. 9(d). Together with the carbochlorination efficiency and XRD results of the fly ash, the SEM image indicated that carbochlorination of the fly ash was completed within 120 min.

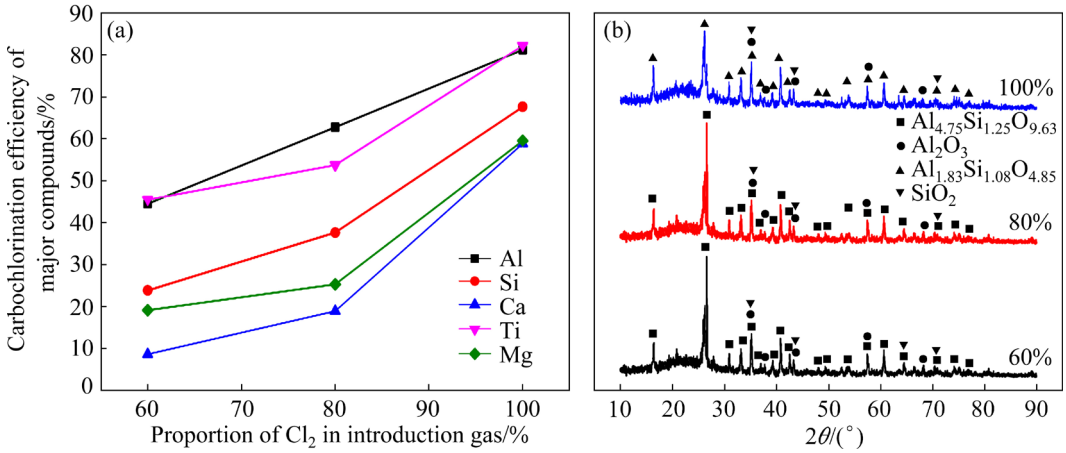

Fig. 8 Carbochlorination efficiency (a) and XRD patterns (b) of fly ash with various proportions of Cl_2

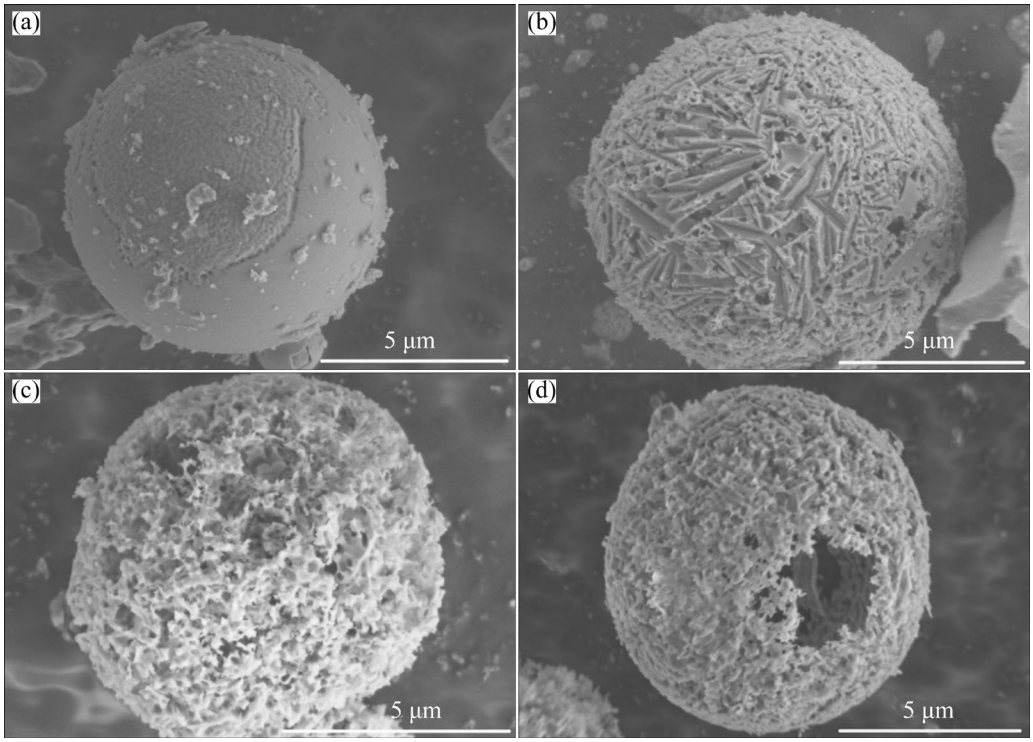

Fig. 9 SEM images of carbochlorination residues produced with different carbochlorination time: (a) 15 min; (b) 30 min; (c) 60 min; (d) 120 min

3.4 Mechanism for fly ash carbochlorination

Based on the analysis presented above, a mechanism for carbochlorination of the fly ash is depicted in Fig. 10.

As shown in Fig. 10, the chlorine gas initially contacted the fly ash and carbon in the pellets. The aluminum and silicon in the mullite phase ($Al_6Si_2O_{13}$) underwent chlorination reactions, resulting in the formation of $AlCl_3$ and $SiCl_4$ and the mullite mesophase ($Al_{4.75}Si_{1.25}O_{9.63}$). The mullite mesophase ($Al_{4.75}Si_{1.25}O_{9.63}$) was subsequently chlorinated to form a new mullite mesophase ($Al_{1.83}Si_{1.08}O_{4.85}$). Al_2O_3, SiO_2, CaO, TiO_2, and MgO in the fly ash were chlorinated to form $AlCl_3$, $SiCl_4$, $CaCl_2$, $TiCl_4$, and $MgCl_2$, respectively. $MgCl_2$, $CaCl_2$, and unreacted oxides remained in the residues for further recycling treatment. $AlCl_3$, $SiCl_4$, and $TiCl_4$ were carried out of the furnace by the flowing gas. Most of the $AlCl_3$ was efficiently collected in the condenser, while $SiCl_4$ and $TiCl_4$ were enriched in the tail gas flow due to the relatively low melting and boiling points. The mechanism for carbochlorination of the fly ash can be expressed as follows:

$$Al_6Si_2O_{13}(s)+C(s)+Cl_2(g)\rightarrow Al_{4.75}Si_{1.25}O_{9.63}(s)+C(s)+Cl_2(g)+AlCl_3(g)+SiCl_4(g)+CO(g)\rightarrow Al_{1.83}Si_{1.08}O_{4.85}(s)+AlCl_3(g)+SiCl_4(g)+CO(g) \quad (6)$$

$$Al_2O_3(s)+C(s)+Cl_2(g)\rightarrow AlCl_3(g)+CO(g) \quad (7)$$

$$SiO_2(s)+C(s)+Cl_2(g)\rightarrow SiCl_4(g)+CO(g) \quad (8)$$

$$TiO_2(s)+C(s)+Cl_2(g)\rightarrow TiCl_4(g)+CO(g) \quad (9)$$

$$MgO(s)+C(s)+Cl_2(g)\rightarrow MgCl_2(s)+CO(g) \quad (10)$$

$$CaO(s)+C(s)+Cl_2(g)\rightarrow CaCl_2(s)+CO(g) \quad (11)$$

3.5 Characterization of carbochlorination products

After the carbochlorination process, a condensation recovery unit was employed to separate the carbochlorination products. The composition of the carbochlorination products in the condenser was analyzed with XRF, XRD, and SEM, and the results are presented in Table 3, Figs. 11 and 12, respectively.

As shown in Table 3, Cl, O, and Al contents in the product were 70.18%, 13.80%, and 12.19 wt.%, respectively, which were significantly higher than the contents of Si, Fe, and Ti. These results confirmed that Al and Cl were enriched as $AlCl_3$.

Figure 11 shows the XRD patterns of the carbochlorination products removed from the condenser. The principal phases were anhydrous aluminum chloride ($AlCl_3$) and aluminum chloride hexahydrate ($AlCl_3·6H_2O$). The presence of $AlCl_3·6H_2O$ was attributed to the absorption of H_2O from the surrounding atmosphere during collection and analyses.

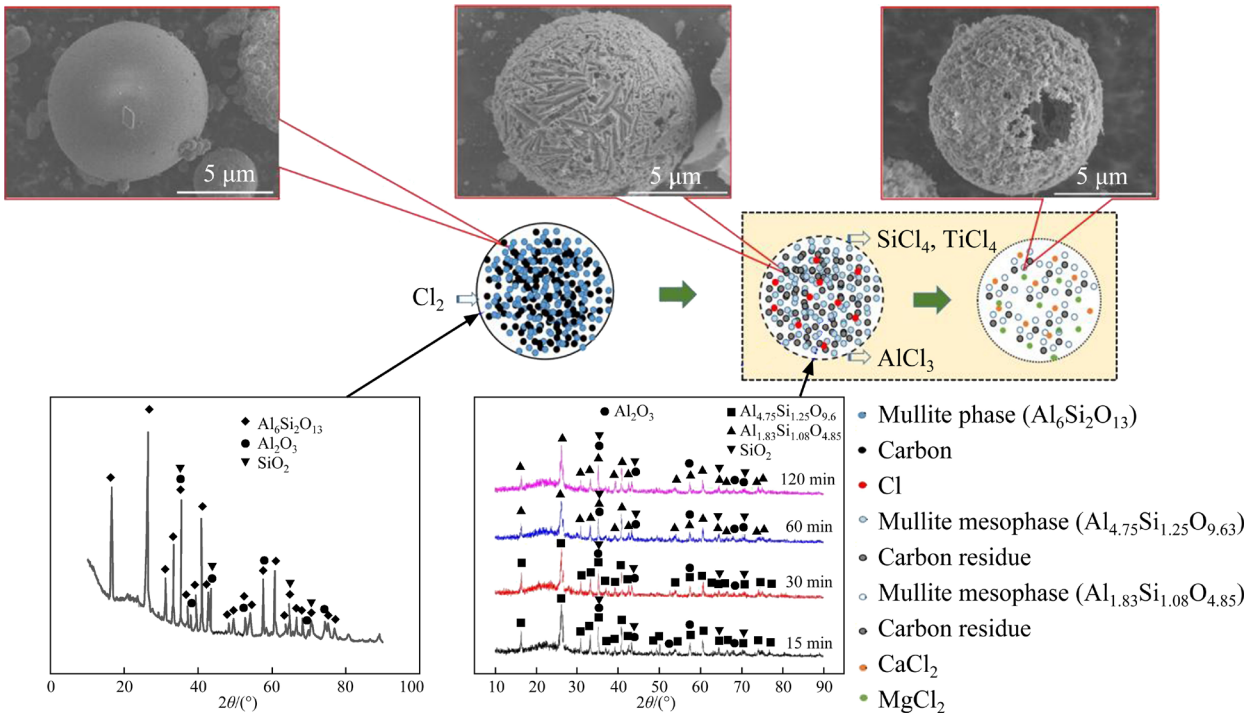

Fig. 10 Schematic showing mechanism for carbochlorination of fly ash

Table 3 Main components of carbochlorination product (wt.%)

Cl	O	Al	Si	Fe	Ti	Other
70.18	13.80	12.19	0.05	0.70	0.35	2.73

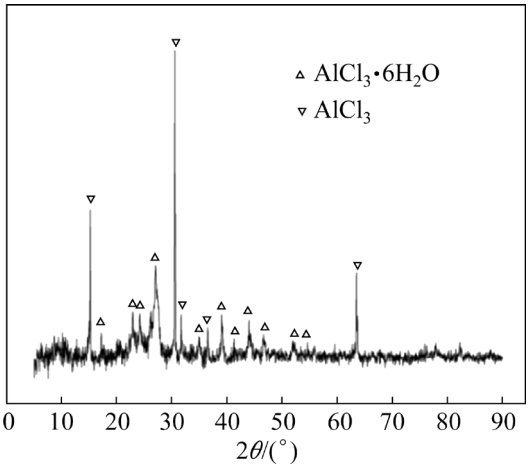

Fig. 11 XRD patterns for carbochlorination products

The SEM image and EDS result for the products are shown in Fig. 12. The carbochlorination products in Fig. 12(a) exhibited tabular morphologies due to the condensation conditions. Additionally, the O, Al, and Cl distributions in the products indicated the simultaneous accumulation of these elements in the form of $AlCl_3$ and $AlCl_3·6H_2O$.

4 Conclusions

(1) The thermodynamic analysis revealed that to achieve efficient carbochlorination of the fly ash, it is essential to carry out the carbochlorination reactions at temperatures of 700−1000 °C.

(2) With the optimal conditions, including temperature of 950 °C, time of 60 min, pellet diameters of 4−6 mm, carbon content of 27.0 wt.%, and gas flow rate of 0.30 L/min with a chlorine proportion of 100%, the carbochlorination efficiency for Al, Si, Ca, Ti, and Mg in the fly ash exceeded 81.18%, 67.62%, 58.87%, 82.15%, and 59.53%, respectively.

(3) The XRD patterns revealed that the aluminum and silicon in the mullite phase ($Al_6Si_2O_{13}$) underwent initial chlorination, resulting in the formation of a mullite mesophase ($Al_{4.75}Si_{1.25}O_{9.63}$) and subsequent transformation into a new mullite mesophase ($Al_{1.83}Si_{1.08}O_{4.85}$). These findings were consistent with the carbochlorination efficiency of the fly ash and SEM images of the carbochlorination residues.

(4) After the carbochlorination process, Al was efficiently collected from the condenser as $AlCl_3$, while $SiCl_4$ and $TiCl_4$ were enriched in the exhaust gas. In contrast, $MgCl_2$, $CaCl_2$, and unreacted oxides remained in the residues for further recycling.

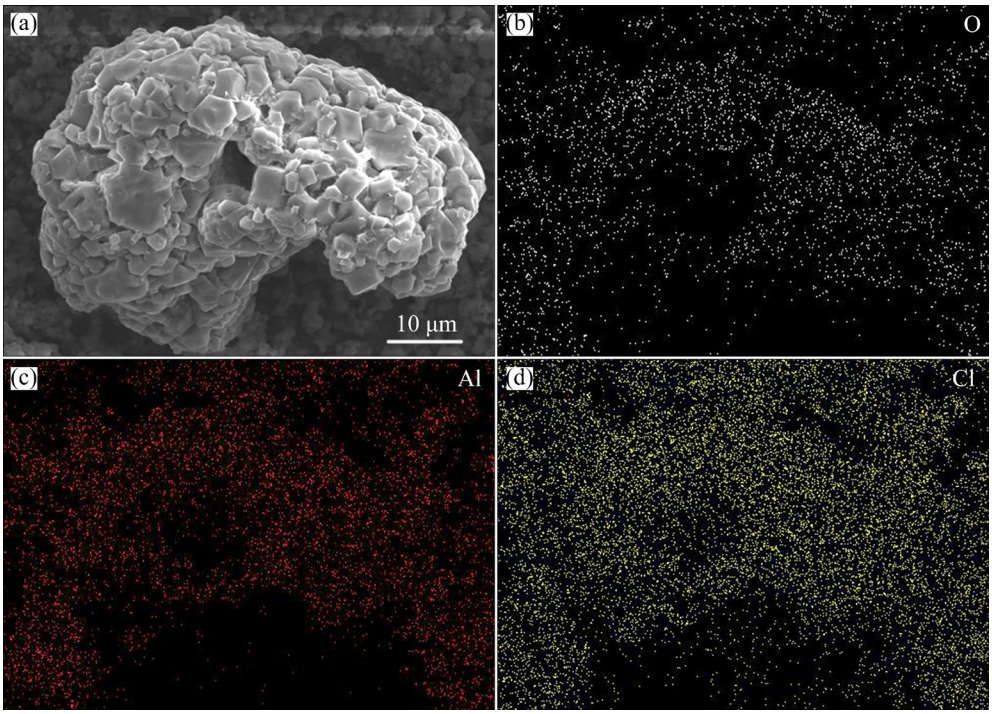

Fig. 12 SEM image (a) and EDS results (b−d) for products

CRediT authorship contribution statement

Long WANG: Conceptualization, Funding Acquisition, Methodology, Software, Investigation, Formal analysis, Writing − Original, Writing − Review & editing; **Xin-xin ZHAO:** Resources, Supervision, Writing − Review & editing; **Zi-mu ZHANG:** Data Curation, Writing − Original draft; **Ting-an ZHANG:** Conceptualization, Funding acquisition, Resources, Supervision, Writing − Review & editing; **Guo-zhi LÜ:** Software, Validation; **Zhi-he DOU:** Resources, Supervision; **Ai-chun ZHAO:** Investigation, Data curation; **Xi-yu ZHANG:** Software, Formal analysis.

Declaration of competing interest

The authors declare that they have no known competing financial interests or personal relationships that could have appeared to influence the work reported in this paper.

Acknowledgments

The authors gratefully acknowledge the National Natural Science Foundation of China (Nos. 52304364, U1710257), and the financial support of the National Key Research and Development Program of China (No. 2022YFB3504502).

References

[1] MA Yi-qian, STOPIC S, XAKALASHE B, NDLOVU S, FORSBERG K, FRIEDRICH B. A cleaner approach for recovering Al and Ti from coal fly ash via microwave-assisted baking, leaching, and precipitation [J]. Hydrometallurgy, 2021, 206: 105754.

[2] WANG Long, ZHANG Ting-an, LV Guo-zhi, DOU Zhi-he, ZHANG Wei-guang, ZHANG Jing-zhong, NIU Li-ping, LIU Yan. Carbochlorination of alumina and silica from high-alumina fly ash [J]. Minerals Engineering, 2019, 130: 85−91.

[3] WANG Long, ZHANG Ting-an, LV Guo-zhi, DOU Zhi-he, SUN Wei-hua, ZHANG Wei-guang, NIU Li-ping, ZHANG Zi-mu. Titanium extraction from fly ash by carbochlorination [J]. JOM, 2019, 71: 4624−4630.

[4] BAI Guang-hui, TENG Wei, WANG Xiang-gang, QIN Jin-guo, XU Peng, LI Peng-cheng. Alkali desilicated coal fly ash as substitute of bauxite in lime-soda sintering process for aluminum production [J]. Transactions of Nonferrous Metals Society of China, 2010, 20(Suppl.): 169−175.

[5] AHMARUZZAMAN M. A review on the utilization of fly ash [J]. Progress in Energy and Combustion Science, 2010, 36: 327−363.

[6] RUI Hong-ming, ZHANG Li-cheng, LI Li-juan, ZHU Li-xia. Solvent extraction of lithium from hydrochloric acid leaching solution of high-alumina coal fly ash [J]. Chemical Physics Letters, 2021, 771: 138510.

[7] WANG Ruo-chao, ZHAI Yu-chun, NING Zhi-qiang, MA Pei-hua. Kinetics of SiO_2 leaching from Al_2O_3 extracted slag of fly ash with sodium hydroxide solution [J]. Transactions of Nonferrous Metals Society of China, 2014, 24: 1928−1936.

[8] YANG Chen-nian, ZHANG Jian-bo, LI Shao-peng, LI Hui-quan, HOU Xin-juan, ZHU Gan-yu. Mechanisms of mechanochemical activation during comprehensive utilization of high-alumina coal fly ash [J]. Waste Management, 2020, 116: 190−195.

[9] LIU Chun-li. Basic research on aluminum-silicon separation of high alumina flu ash [D]. Beijing: Institute of Process Engineering, University of Chinese Academy of Sciences, 2019. (in Chinese)

[10] GONG Yan-bing, SUN Jun-min, ZHANG Yin-min, ZHANG Yong-feng, ZHANG Ting-an. Dependence on the distribution of valuable elements and chemical characterizations based on different particle sizes of high alumina fly ash [J]. Fuel, 2021, 291: 120225.

[11] MA Zhi-bin, ZHANG Sen, ZHANG Hui-rong, CHENG Fang-qin. Novel extraction of valuable metals from circulating fluidized bed-derived high-alumina fly ash by acid−alkali-based alternate method [J]. Journal of Cleaner Production, 2019, 230: 302−313.

[12] MOHEBBI M, RAJABIPOUR F, MADADIAN E. A framework for identifying the host phases in coal-derived fly ash [J]. Fuel, 2022, 314: 122806.

[13] CAO Peng-xu, LI Guang-hui, JIANG Hao, ZHANG Xin, LUO Jun, RAO Ming-jun, JIANG Tao. Extraction and value-added utilization of alumina from coal fly ash via one-step hydrothermal process followed by carbonation [J]. Journal of Cleaner Production, 2021, 323: 129174.

[14] ZHOU Chun-cai, LI Chen, LI Wen-wen, SUN Jin-ke, LI Quan-zhong, WU Wen-tao, LIU Gui-jian. Distribution and preconcentration of critical elements from coal fly ash by integrated physical separations [J]. International Journal of Coal Geology, 2022, 261: 104095.

[15] LIU Chun-li, MA Shu-hua, DING Jian, LUO Yang, ZHENG Shi-li, ZHANG Yi. Kinetics of decomposition of mullite and corundum in coal fly ash under highly alkaline condition [J]. Transactions of Nonferrous Metals Society of China, 2019, 29: 868−875.

[16] ZHANG Yu-juan, SUN Jun-min, LV Guo-zhi, ZHANG Ting-an, GONG Yan-bing. Kinetics of alumina extraction from coal gangue by hydrochloric acid leaching [J]. Transactions of Nonferrous Metals Society of China, 2023, 33: 1932−1942.

[17] LI Da, JIANG Kai-xi, JIANG Xun-xiong, ZHAO Feng, WANG Sheng-dong, FENG Lin-yong, ZHANG Deng-gao. Improving the A/S ratio of pretreated coal fly ash by a two-stage roasting for Bayer alumina production [J]. Fuel, 2022, 310: 122478.

[18] WANG Hong-yang, ZHANG Xiao-xue, YANG Si-yuan, LIU Cheng, LUO Li-qun. Separation of alumina and silica from metakaolinite by reduction roasting−alkaline leaching process: Effect of $CaSO_4$ and CaO [J]. Transactions of Nonferrous Metals Society of China, 2022, 32, 999−1009.

[19] SANGITA S, NAYAK N, PANDA C R. Extraction of aluminium as aluminium sulphate from thermal power plant fly ashes [J]. Transactions of Nonferrous Metals Society of

China, 2017, 27: 2082−2089.
[20] TRIPATHY A K, BEHERA B, AISHVARYA V, SHEIK A R, DASH B, SARANGI C K, TRIPATHY B C, SANJAY K, BHATTACHARYA I N. Sodium fluoride assisted acid leaching of coal fly ash for the extraction of alumina [J]. Minerals Engineering, 2019, 131: 140−145.
[21] RAMPOU M, NDLOVU S, SHEMI A. Purification of coal fly ash leach liquor for alumina recovery using an integrated precipitation and solvent extraction process [J]. Journal of Sustainable Metallurgy, 2017, 3: 782−792.
[22] LI Jian, GAO Jian-ming, GUO Yan-xia, CHENG Fang-qin. Energy-efficient leaching process for preparation of aluminum sulfate and synergistic extraction of Li and Ga from circulating fluidized bed fly ash [J]. Energy Sources, Part A: Recovery, Utilization, and Environmental Effects, 2022, 44(2): 4398−4410.
[23] SAHAYAM A C, VENKATESWARLU G, THANGAVELA S. Leaching of gallium from coal fly ash, alumina and sediment samples with an acid mixture for its determination by ICP-OES [J]. Atomic Spectroscopy, 2021, 42(1): 32−35.
[24] GAO Ya-jing, LIANG Kai, GOU Yi, WEI Shun-an, SHEN Wei-feng, CHENG Fang-qin. Aluminum extraction technologies from high aluminum fly ash [J]. Reviews in Chemical Engineering, 2021, 37(8): 885−906.
[25] ADELMAN D J, BURNET G. Carbochlorination of metal oxides with phosgene [J]. AIChE Journal, 1987, 33(1): 64−69.
[26] VETCHINKINA T N, BALMAEV B G. Chlorination of alumina obtained from nepheline concentrate processing and comparative assessment of the complete aluminum production cycle [J]. Inorganic Materials: Applied Research, 2019, 10: 1249−1253.
[27] LANDSBERG A. Chlorination kinetics of aluminum bearing minerals [J]. Metallurgical Transactions B, 1975, 6: 207−214.
[28] WANG Long, ZHANG Ting-an, LV Guo-zhi, ZHANG Jing-zhong, DOU Zhi-he, ZHANG Wei-guang, NIU Li-ping, LIU Yan. Investigation of the carbochlorination mechanism of mullite from fly ash [J]. Metallurgical and Materials Transactions B, 2018, 49: 2835−2845.
[29] ZHANG Ting-an, DOU Zhi-he, LIU Yan, LV Guo-zhi, WANG Long, NIU Li-ping, FU Da-xue, ZHAO Qiu-yue, ZHANG Wei-guang. A comprehensive utilization method for preparing alumina from fly ash by pellet chlorination electrolysis [P]. China, ZL201710324790.2, 2018-10-23. (in Chinese)

高铝粉煤灰中有价元素的碳热氯化协同提取分离

王 龙[1]，赵昕昕[1]，张子木[2]，张廷安[1]，吕国志[1]，豆志河[1]，赵爱春[3]，张溪雨[1]

1. 东北大学 多金属共生矿生态化冶金教育部重点实验室，沈阳 110819；
2. 沈阳化工大学 机械工程学院，沈阳 110142；
3. 太原科技大学 材料科学与工程学院，太原 030024

摘 要：提出一种高铝粉煤灰有价组元协同提取分离的新工艺。热力学分析结果表明，粉煤灰的碳热氯化反应在700~1000 ℃之间进行可以获得较好的氯化性能。实验结果表明，在优化条件下，粉煤灰中铝、硅、钙、钛和镁的碳热氯化效率分别达到81.18%、67.62%、58.87%、82.15%和59.53%。XRD分析结果表明，在碳热氯化反应过程中，莫来石相($Al_6Si_2O_{13}$)中的铝和硅被氯化，从而形成莫来石中间相($Al_{4.75}Si_{1.25}O_{9.63}$和$Al_{1.83}Si_{1.08}O_{4.85}$)。碳热氯化反应完成后，铝以氯化铝形式在冷凝器中冷凝沉积，氯化硅和氯化钛在尾气中富集，氯化钙、氯化镁和未反应的氧化物留在残留物中进一步循环利用。

关键词：高铝粉煤灰；碳热氯化；热力学；协同提取；机理

(Edited by Xiang-qun LI)